

Article

Investigating the Timing of Carbonate Precipitations and Their Potential Impact on Fossil Preservation in the Hell Creek Formation

Daigo Yamamura

Miles Community College, 2715 Dickinson Street, Miles City, MT 59301, USA; yamamurad@milescc.edu

Abstract: Because fossilized skeletal remains and enclosing sedimentary rocks experience similar diagenetic conditions (i.e., temperature, pressure, and pore fluid interaction), enclosing sedimentary rocks may provide insight into bone diagenesis. A fossil assemblage, including in situ dinosaur fossils, was discovered in Makoshika State Park near Glendive, MT. Fossil-bearing sandstone is a crevasse splay deposit, and fossils show no sorting or preferred orientation. Bone-bearing sandstone exhibits evidence for intense diagenesis, suggesting a maximum temperature of ~90 °C. Concretion associated with fossils includes two distinctive matrices: dark- and light-colored matrices. Another concretion was found in channel sandstone near the base of the outcrop. These carbonate phases have distinctive isotopic compositions; $\delta^{13}\text{C}$ values for dark-colored matrices, light-colored matrices, and spheroidal concretion are -7.5 , 2.1 , and -22.4‰ (VPDB), respectively, and their $\delta^{18}\text{O}$ values are 16.4 , 25.9 , and 17.8‰ (VSMOW), respectively. In contrast, fossilized bone $\delta^{13}\text{C}$ and $\delta^{18}\text{O}$ values were -4.4‰ (VPDB) and 20.6‰ (VSMOW), respectively, suggesting fractionation with pore fluid was limited. Early carbonate precipitation evidenced by grain coating may have reduced interaction between pore fluids and fossils. Although concretion formation and permineralization do not appear to directly aid in fossil preservation, concretions preserve valuable evidence for diagenetic history.

Keywords: diagenesis; concretion; fossilization; Hell Creek Formation; crevasse splay



Citation: Yamamura, D. Investigating the Timing of Carbonate Precipitations and Their Potential Impact on Fossil Preservation in the Hell Creek Formation. *Minerals* **2024**, *14*, 1133. <https://doi.org/10.3390/min14111133>

Academic Editor: Olev Vinn

Received: 20 September 2024

Revised: 22 October 2024

Accepted: 26 October 2024

Published: 9 November 2024



Copyright: © 2024 by the author. Licensee MDPI, Basel, Switzerland. This article is an open access article distributed under the terms and conditions of the Creative Commons Attribution (CC BY) license (<https://creativecommons.org/licenses/by/4.0/>).

1. Introduction

As fossils and enclosing sedimentary rocks experience similar diagenetic environments, studying diagenetic indicators of enclosing sedimentary rocks would aid in understanding the physical condition fossils have experienced throughout diagenesis. Advancements in analytical techniques in the last two decades have provided opportunities to study fossils in new ways. Schweitzer et al. [1], Pan et al. [2], Bailleul et al. [3], and other studies have reported discoveries of biomolecules. Owing to the advancement of molecular analyses, researchers have identified the color of the periscapular spine of ankylosaur [4] and the feathers of Cretaceous birds [2] and the evolutionary trend in dinosaur metabolism [5]. Stable isotope geochemistry has been employed for investigating trophic structure [6–8] and investigating paleoclimate [9,10]. While these new studies have provided valuable paleontological insights, the surrounding sedimentary rocks rarely attract scientists' attention. In an effort to understand bone diagenesis in the Hell Creek Formation, enclosing sandstone and associated concretions were analyzed along with fossils.

Carbonate cements have a wide variety in terms of their chemistry and geometry, and cementation can take place in various stages of diagenesis [11]. Carbonates are the predominant cement in sandstones, and reduction in the porosity and permeability of sandstone may aid in the preservation of fossils by limiting the interaction between biological remains and pore fluids. Carbonate concretions occasionally yield extraordinary preservation [12], and permineralization is considered one of the processes to enhance the preservation of bones [13]. In an earlier investigation of molecular paleontology, cements in the enclosing sandstone matrix have been invoked as an entombing medium facilitating preservation

of vertebrate skeletal material by isolation from contact with pore fluid [14]. As concretions' geometry and stable isotope compositions are often useful for characterizing their origin [15], analyzing concretions may reveal diagenetic conditions of enclosing sandstone throughout diagenetic history.

Diagenesis comprises the post-burial physical, chemical, and biological changes to sediment and enclosed skeletal remains during lithification and fossilization [16,17]. Because burial and exhumation of sediments and enclosed skeletal remains take place together, physical conditions such as pressure, temperature, and interaction with pore fluid are likely similar for fossils and enclosed sedimentary rocks. Thus, determining the diagenetic pathway for the enclosing sandstone helps decipher the diagenetic pathway for the skeletal remains. Such investigation includes analyzing modification of pore spaces/fabric and diagenetic mineral precipitation/alteration in both enclosing sandstone and skeletal remains.

To investigate the relationship between sandstone diagenesis and fossilization, finding in situ fossils is essential. Additionally, the presence of concretion would provide additional information about the diagenesis of enclosing sedimentary rocks. Because of easy access and potential for finding in situ fossils, the Hell Creek Formation was selected for this study. Previous studies of the Hell Creek Formations reported biomolecular preservation in dinosaur bones [1,18]. Fricke and Pearson [19] supported the niche partitioning in the Hell Creek fauna using stable isotope compositions of dinosaur tooth enamel and gar scale. During et al. [20] also used stable isotope compositions of sturgeon and paddlefish fossils to narrow down the season of the K-Pg extinction event. Therefore, understanding sandstone diagenesis in the Hell Creek Formation may have a broad impact on various aspects of paleontological research.

This study focuses on (1) understanding the history of carbonate precipitation in a fossil assemblage in the Hell Creek Formation and (2) assessing its impact on fossil preservation. Diagenetic events were investigated using thin-section petrography, and stable isotope compositions aided in interpreting the timing of carbonate precipitation.

2. Geologic Setting

2.1. Hell Creek Formation Near Glendive, MT

The Upper Cretaceous Hell Creek and overlying Paleocene Tullock member of the Fort Union Formations were deposited as a prograding wedge of clastic sediment associated with the retreat of the Western Interior Seaway [21,22]. The Hell Creek Formation is exposed along the Cedar Creek Anticline in southeast Montana (Figure 1). The Hell Creek Formation overlies the Colgate Member of the Fox Hills Sandstone [23], and the upper boundary of the Hell Creek Formation (K-Pg boundary) is defined by the stratigraphically lowest lignite bed above the highest in situ dinosaur remains [24]. The Hell Creek Formation sediments are volcanoclastic sediments derived from the Cordilleran highland to the west [25]. The estimated duration of deposition represented by the Hell Creek Formation varies from 1.36 to 2.5 million years [26,27]. Zaleha [25] states that (1) the Hell Creek Formation in the Glendive area is composed of interbedded floodplain mudrock and channel sandstone and (2) lithofacies observed in the study area are comparable to the five lithofacies described by Fastovsky [22], which were later expanded to nine lithofacies by Sheehan et al. [28].

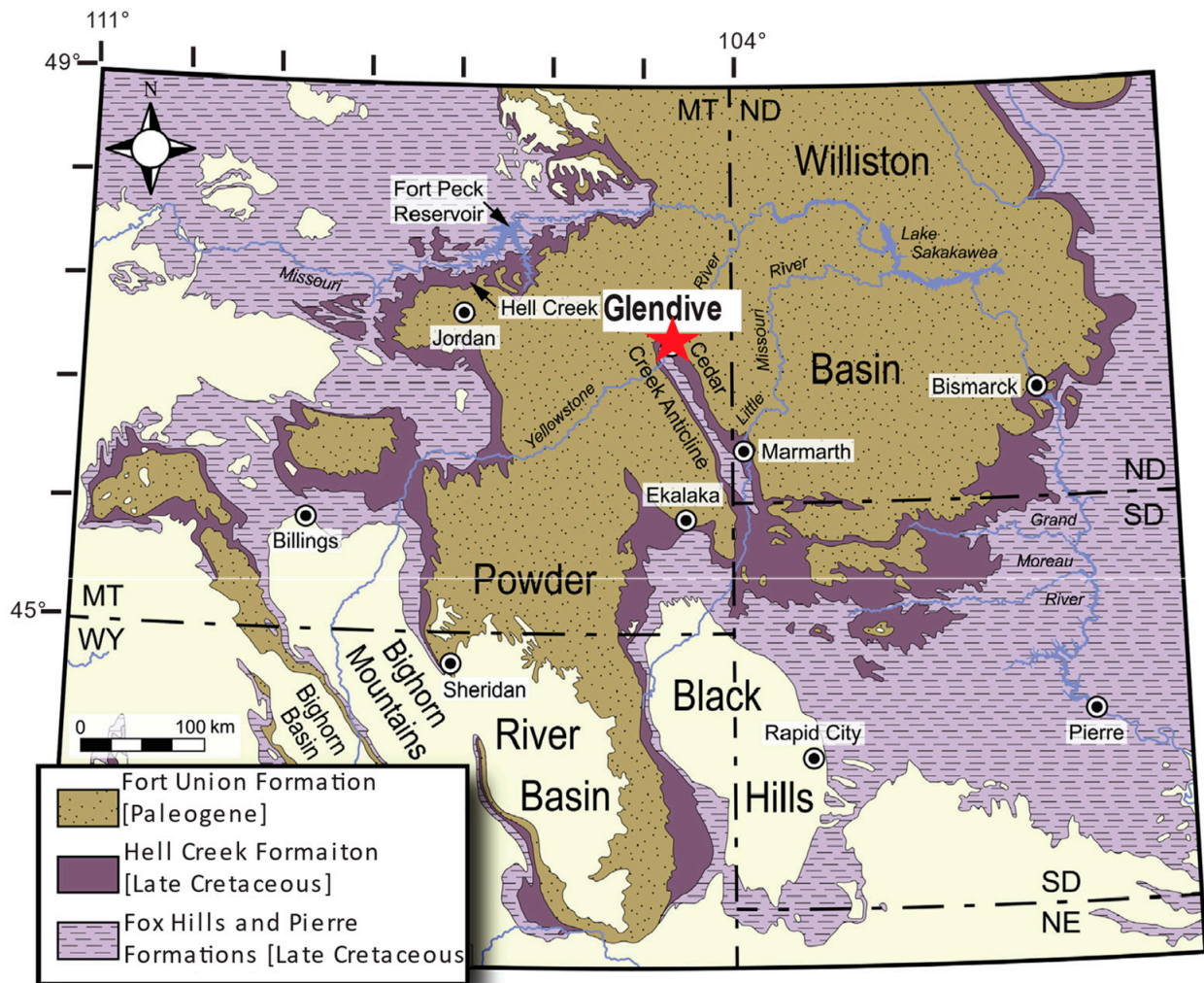


Figure 1. Geologic map of the Late Cretaceous to Paleogene formations, northern Great Plains, USA. Modified from Fastovsky and Bercovici [29]; the original map is from Johnson et al. [30]. The red star indicates the study area. MT: Montana, ND: North Dakota, WY: Wyoming, SD: South Dakota, NE: Nebraska.

2.2. Fossil Assemblage

A fossil assemblage was discovered on a hill slope within Makoshika State Park (Glendive, MT, USA). Based on the proximity to the known K-Pg boundary near the Kinney Coulee Trail, the fossil assemblage is roughly 20 m below the K-Pg boundary (Figure 2). Fossils discovered include disarticulated bones of multiple species and elements including hadrosaur (teeth, ossified tendon, and humerus), ceratopsids (hone core and teeth), champsosaur (femur), turtle (shell fragments and phalange), small theropod (teeth), crocodile (teeth and dermal bones), fish (ganoine scales and vertebra), and bird (metatarsal). Fossils were found in a single sandstone bed and do not exhibit sorting (ranges from 7 mm to 80 cm) or preferred orientation. While carbonate concretion partially covered and permineralized large bones, carbonate cements were not associated with small fossils. Large bones, including femur and rib fragments, in this study were only partially exposed. Thus, fossils are still in contact with the original host rock.

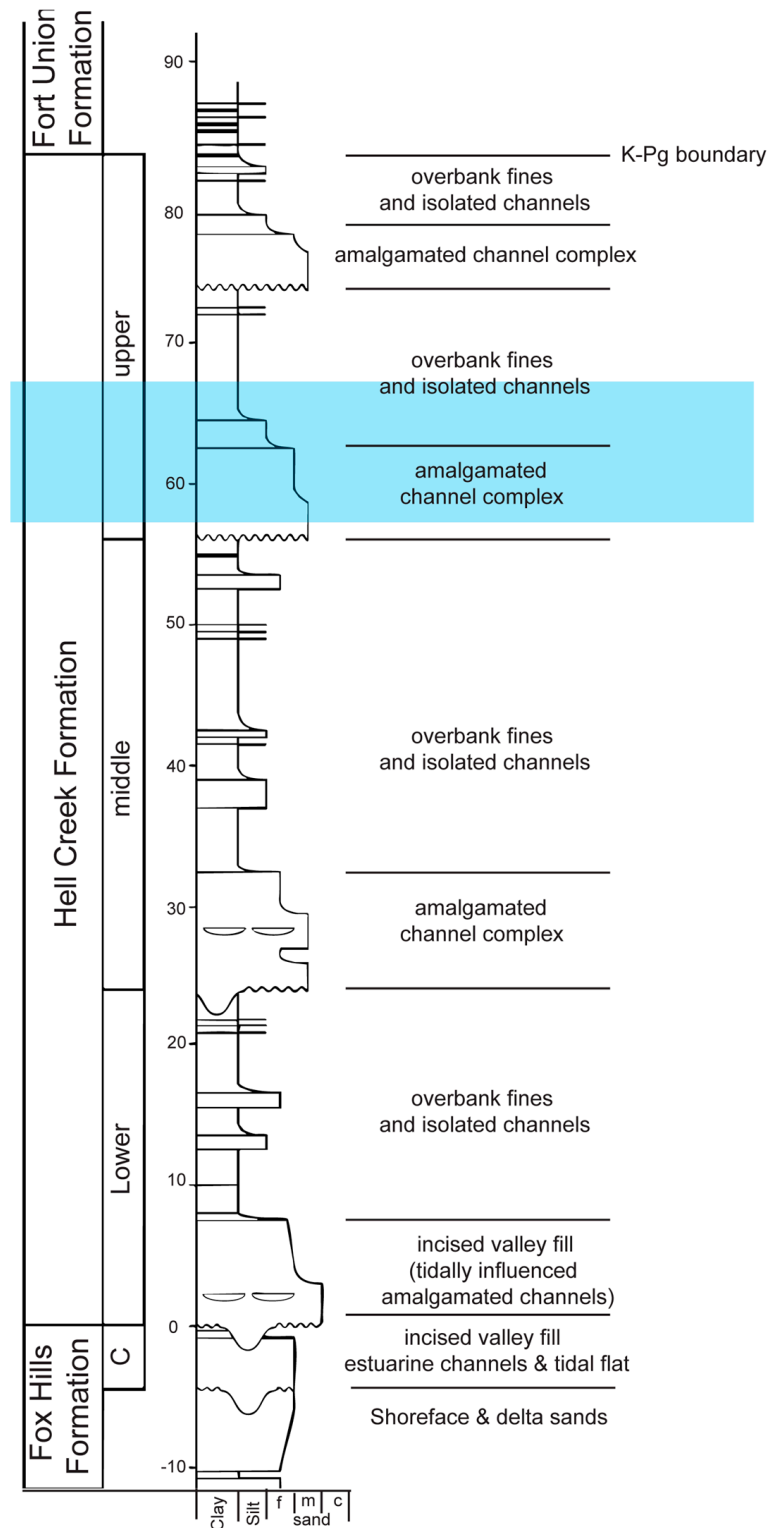


Figure 2. Representative stratigraphic column of the Hell Creek Formation and the equivalent sequence to this study (highlighted in blue). Modified from Fowler [31].

2.3. Regional Geology and Diagenetic Stages

Although early studies do not have consistent terminologies in diagenetic stages, the terms “eogenesis”, “mesogenesis” and “telogenesis” in this study will refer to the stages of shallow burial, deep burial, and exhumation/uplift, respectively. Eogenesis in this study refers to the diagenetic stage from the deposition/burial to the zone of

intense diagenesis [32]. The zone of intense diagenesis is characterized by diagenetic reactions, including clay diagenesis, carbonate dissolution, and feldspar dissolution, and the temperature ranges from 80 to 120 °C [32]. Mesogenesis in this study refers to the diagenetic stage from intense diagenesis to regional uplift. Regional epeirogenic uplift in the Late Oligocene to Early Miocene stages initiated erosion of this area, the basin-fill model based on thermal parameters from Cretaceous rocks and oil well temperature data suggest that net aggradation to the present day was approximately 2.7 km [33]. Thus, fossils and enclosing sandstone reached maximum burial depth before the Late Oligocene to Early Miocene stages. In this study, telogenesis refers to the diagenetic stage after the epeirogenic uplift.

3. Materials and Methods

3.1. Section Measurement

The section measurement included trenching near the fossil assemblage (Figure 3) for lithologic observation (i.e., rock type, sedimentary structures, etc.) and thickness measurement of each unit by using a 1.5 m Jacob's staff. Rock samples for petrography were collected 5–10 cm deep in the quarry and the channel sandstone at the base in order to minimize the effect of surface weathering. Additional samples collected for petrography include fossilized dinosaur bone (fragmentary femur and rib of ornithischian dinosaur) and concretion formed around dinosaur bone. A spheroidal concretion found in the channel sandstone near the base of the outcrop was also collected for stable isotope composition analysis.



Figure 3. Field photo showing the outcrop studied. Black line indicates the location of the trench for stratigraphic analysis. The black arrow indicates the location of the fossil assemblage studied. The scale bar is added based on a tape measure on the foreground of the photograph, and thickness of the beds on upper section appear thinner due to the slope of the outcrop.

3.2. Thin Section Petrography

Petrographic thin sections were prepared for (1) the channel sandstone, (2) bone-bearing sandstone, (3) concretions associated with fossils, and (4) dinosaur fossil bones including femur and rib fragments. Concretions were separated from the fossils in a laboratory during the preparation of the fossil specimens. Although the majority of concretion is reddish brown in color, lighter-colored inclusions were found frequently when concretions were cut open. Additionally, both darker- and lighter-colored matrices of concretion reacted

with dilute hydrochloric acid to produce effervescence. Both femur and rib fragments were only partially exposed at the time of discovery, and petrographic samples were taken from the buried portion to avoid modification due to surface weathering. After sorting and initial preparation, fossil and rock samples were sent to Spectrum Petrographics, Inc. for professional thin section preparation. Selected thin sections were stained with K-feldspar stain and Fe-carbonate stains for compositional analysis. In case further analyses were necessary, thin sections were not covered with cover slides.

3.3. Stable Isotope Geochemistry

Small pieces of cortex and cancellous bones were taken from the femur fragment for isotope analysis. After removing potential contamination, fossils were ground into a fine powder with a mortar and pestle. The powdered samples of fossils were treated with calcium acetate solution in order to remove diagenetic calcite following Koch et al. [34].

Because two carbonate phases (i.e., light-colored and dark-colored matrices) were difficult to separate, a dental drill was used to prepare powdered samples of concretions from bone-bearing sandstone. A dental drill was also used for spheroidal concretion from the channel sandstone to avoid sampling from potentially weathered external surfaces.

The isotopic compositions of the powdered samples were analyzed using a Gas Bench II coupled to the Delta Plus XP Isotopic Ratio Mass Spectrometer (IRMS) at the University of Arkansas Stable Isotope Laboratory (UASIL). Instrument stability was monitored using NBS-19, which produced a value of $\delta^{13}\text{C}$ relative to Vienna Pee Dee Belemnite (VPDB) = $1.93 \pm 0.05\%$ 1σ standard deviation and $\delta^{18}\text{O}$ relative to Vienna Standard Mean Ocean Water (VSMOW) = $28.65 \pm 0.11\%$ 1σ standard deviation. Reported true values of NBS-19 are $\delta^{13}\text{C} = 1.95\%$ VPDB and $\delta^{18}\text{O} = 28.65\%$ VSMOW. Two in-house standards are also used for calibration: UASIL-22 and UASIL-23. UASIL-22 returned values of $\delta^{13}\text{C} = -35.60 \pm 0.04\%$ VPDB 1σ standard deviation and $\delta^{18}\text{O} = -17.07 \pm 0.17\%$ VPDB 1σ standard deviation. True values of UASIL-22 are $\delta^{13}\text{C} = -35.60\%$ and $\delta^{18}\text{O} = -17.07\%$. UASIL-23 returned values of $\delta^{13}\text{C} = -0.59 \pm 0.09\%$ VPDB 1σ standard deviation and $\delta^{18}\text{O} = -14.72 \pm 0.12\%$ VPDB. True values of UASIL-23 are $\delta^{13}\text{C} = -0.60\%$ VPDB and $\delta^{18}\text{O} = -14.71\%$ VPDB. The precision was monitored via analysis of NIST 120c Florida phosphate rock ($\text{Ca}_5(\text{PO}_4)_2.5(\text{CO}_3)_{0.5}\text{F}$), producing an average value of $\delta^{13}\text{C} = -6.28 \pm 0.12\%$ VPDB and $\delta^{18}\text{O}$ of $29.09 \pm 0.30\%$ VSMOW.

The carbon isotope compositions of fossils are referred to as $\delta^{13}\text{C}$, and values are reported relative to VPDB. The oxygen isotope compositions of concretion and fossils are referred to as $\delta^{18}\text{O}$ and reported relative to VSMOW; VSMOW is the internationally accepted reference for ^{18}O prepared from distilled seawater by the International Atomic Energy Agency (IAEA).

4. Results

4.1. Stratigraphic Measurement

The measured section includes sandstone, mudrock, and coal deposits (Figure 4). The sandstone at the base of the outcrop exhibits trough cross-stratification and is highly porous. Interlayered sandstone and mudrock overlie the cross-laminated sandstone. Above the interlayered sandstone/mudrock unit, 20 cm to 1 m sandstone and mudrock units repeat. Based on the facies association, the fossil-bearing sandstone was interpreted as a crevasse splay deposit (see Appendix A for detailed facies analysis).

A fossil assemblage was discovered in a sandstone unit roughly 7 m from the base of the outcrop. Two types of carbonate concretions were found throughout the section measured: (1) carbonate nodules/concretions associated with large fossils and (2) spheroidal concretions in channel sandstone at the base of outcrop.

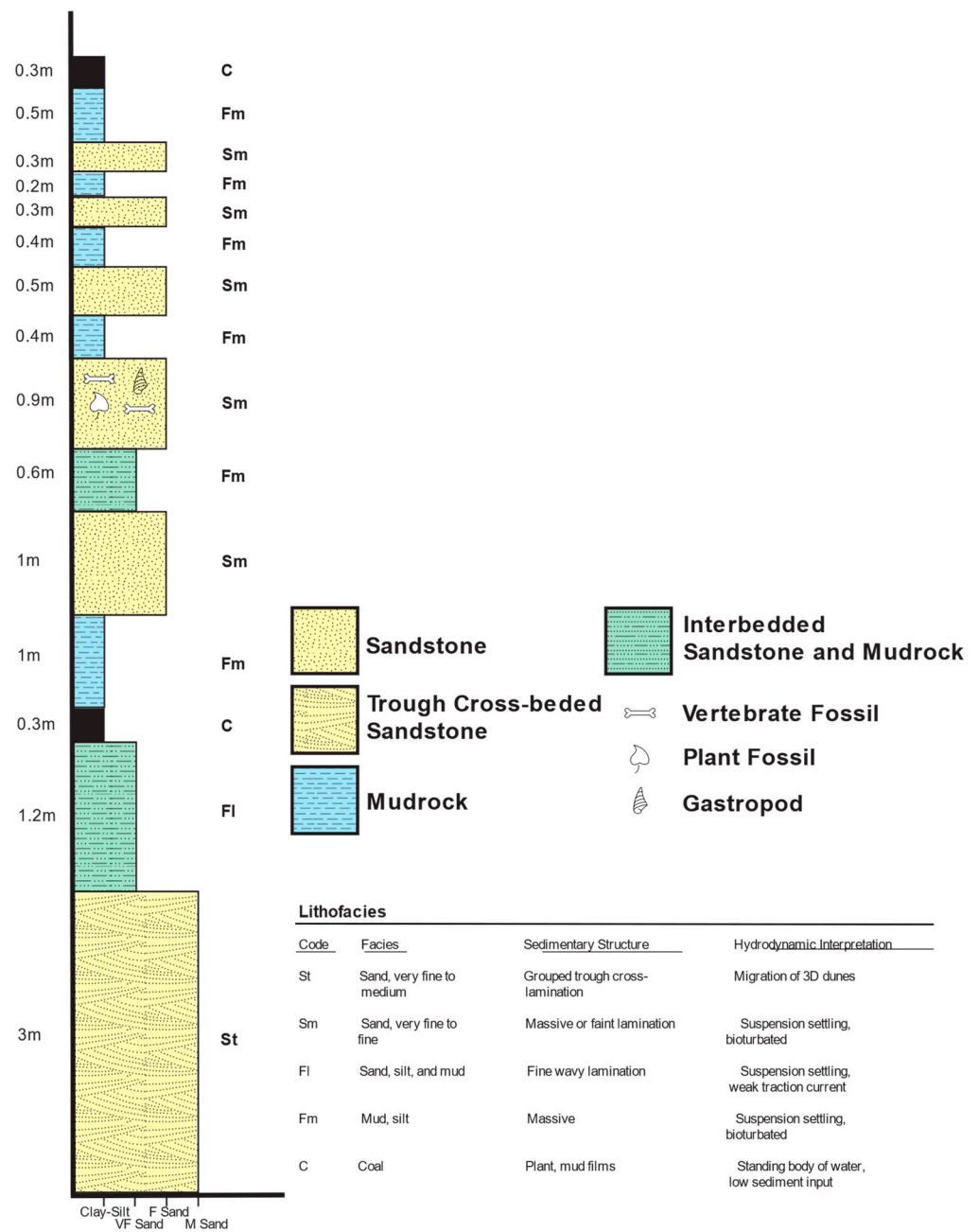


Figure 4. Measured stratigraphic column of the study area. The lower sequence includes channel sandstone and interbedded sandstone and mudrock. Above the first coal layer, sandstone and mudrock beds repeat until another coal layer.

4.2. Fossil Assemblage

Fossils found in this assemblage are isolated and have a wide range in size (1 to 80 cm). Large fossils include a hadrosaur humerus (80 cm long), fragmentary femur (25 cm wide), and rib (20 cm long). Small fossils found include an avian metatarsal, a ceratopsian horn fragment, gar scales, turtle shell fragments and phalange, a champsosaur femur, tooth fragments (theropod, hadrosaur and ceratopsid), and many unidentifiable pieces. All fossil bones were isolated and no articulated bones were discovered. Additionally, plant fossils including carbonized leaf and pine cone, impressions, and gastropod cast were discovered. The sandstone hosting this fossil assemblage was interpreted as a crevasse splay deposit based on the facies association. Isolated bone elements of various taxa,

unsorted nature of fossils, and the presence of plant remains coincide with the depositional environment interpretation.

4.3. Thin Section Petrography

4.3.1. Channel Sandstone

Grain contacts are point-contact and almost float due to grain dissolution. Feldspar grains and volcanic rock fragments are highly altered; skeletonized grains (partial dissolution, Figure 5a) and oversized pores (complete dissolution, Figure 5a) are common. Clay minerals often outline the oversized pores. Some unaltered euhedral potassium feldspar crystals are present in the channel sandstone (Figure 5b). These euhedral potassium feldspar grains are found either within or adjacent to volcanic rock fragments. The exploded fabric of biotite (Figure 5b) indicates early precipitation of calcite, yet carbonate cement is absent in channel sandstone.

The stained thin sections (Figure 5c) exhibit up to 25% of feldspar content. Also, lithic fragments are very common (up to 30%) in the channel sandstone (Figure 5c). Thus, the channel sandstone is a highly porous (up to 50%) feldspathic litharenite. Framework grains include quartz, feldspar, volcanic rock fragments, and accessory minerals including biotite, apatite, and hornblende. Grains are subangular to angular, and some quartz grains show overgrowths.

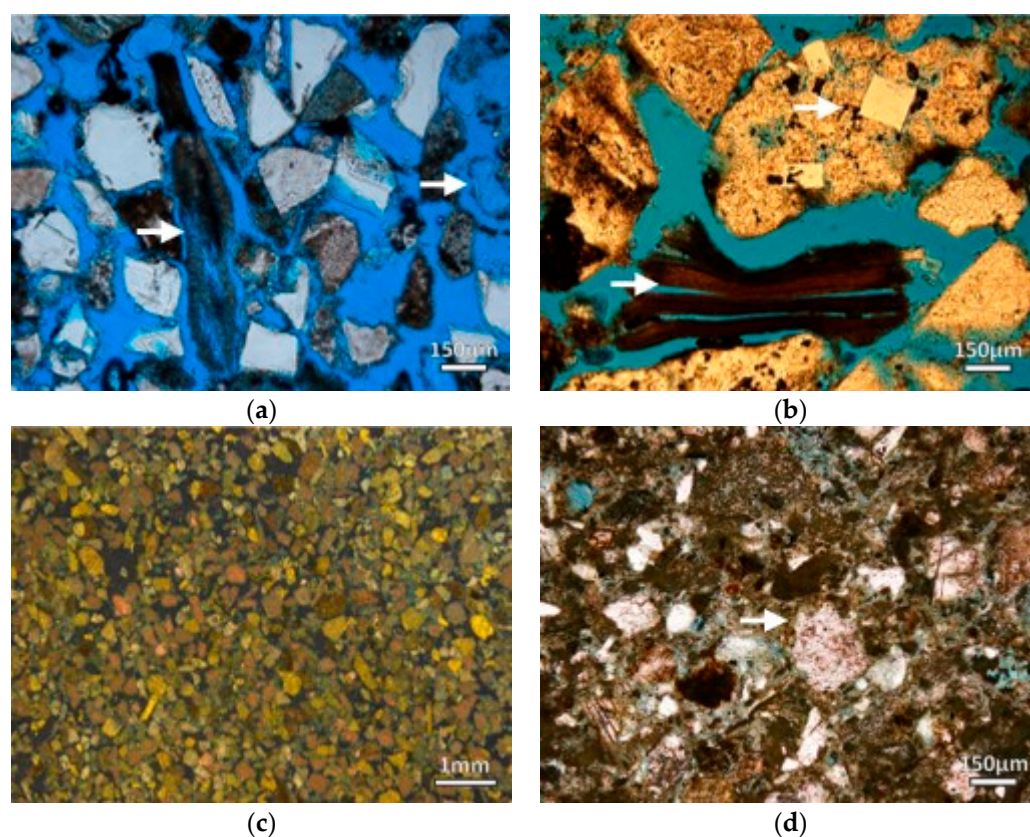


Figure 5. Cont.

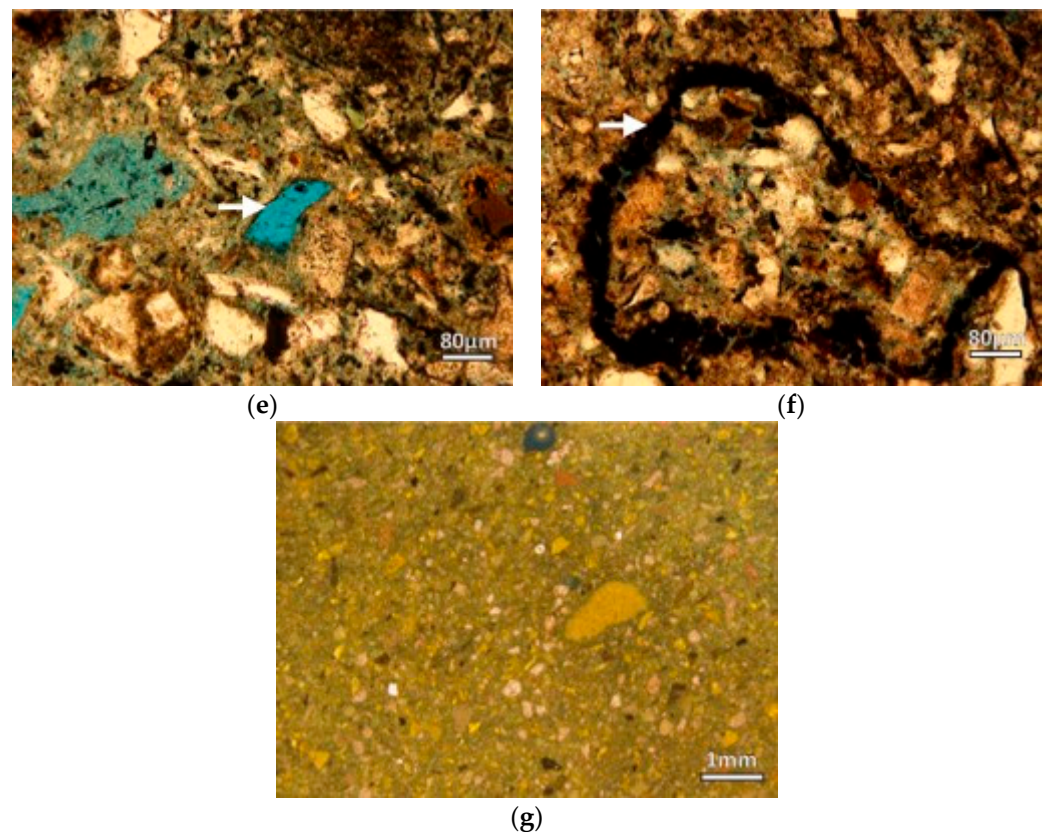


Figure 5. Photomicrographs of the channel sandstone (a–c) and bone-bearing sandstone (d–g). The objective lens used is $2\times$ for (c,g) (scale bar = 1 mm), $10\times$ for (a,b,d) (scale bar = $150\ \mu\text{m}$), and $20\times$ for (e,f) (scale bar = $80\ \mu\text{m}$). All micrographs were captured with plane polar light. Blue epoxy was used to recognize plucked grains versus pore space. Yellow grains on c and g are stained with K-feldspar stain. Characteristic features include (a) arrows indicate a skeletonized grain and complete grain dissolution outlined by clay precipitation prior to dissolution; (b) arrows indicate exploded fabric of biotite crystals and volcanic rock fragment enclosing euhedral crystals of K-feldspar; (c) thin section of channel sandstone stained for K-feldspar, captured with low light condition to visualize the stain; (d) arrow indicates altered feldspar grain commonly found across bone-bearing sandstone; (e) arrow indicates secondary pore created by grain dissolution; (f) arrow indicates outline of pre-existing grain shown by oxide and clay; and (g) thin section of bone-bearing sandstone stained for K-feldspar, captured with low light condition to visualize the stain.

4.3.2. Bone-Bearing Sandstone

Framework grains include quartz, feldspar, and volcanic rock fragments, and accessory minerals include calcite, Fe-oxide (hematite), and other mafic minerals. Feldspar and volcanic rock fragments often have an altered appearance (Figure 5d). Grains are angular to subangular, and grain contacts are point to almost floating. Complete grain dissolution is also observed in bone-bearing sandstone (Figure 5e) but is less frequent than in channel sandstone. Fe-oxide sometimes outlines pre-existing volcanic rock fragments (Figure 5f). The stained section indicates high (up to 25%) feldspar content (Figure 5g). Lithic fragments are also common (up to 30%) in the bone-bearing sandstone (Figure 5g). Thus, the bone-bearing sandstone is a mud-rich feldspathic litharenite. Partial dissolution of grains is very common in the bone-bearing sandstone.

4.3.3. Concretion

Concretions exhibit two distinct phases that are visible without a microscope: light-colored matrices and dark-colored matrices (Figure 6a). Lighter matrices are gray in color and exhibit higher birefringence with polarized light, whereas darker matrices are mostly

opaque to red with single-polar light (with higher light intensity). Based on the partially opaque nature and the color, the dark matrices are composed of multiple mineral phases. Characteristics of the grains included in both matrices are the same; more angular and less altered compared to grains in the bone-bearing sandstone (outside the concretion.)

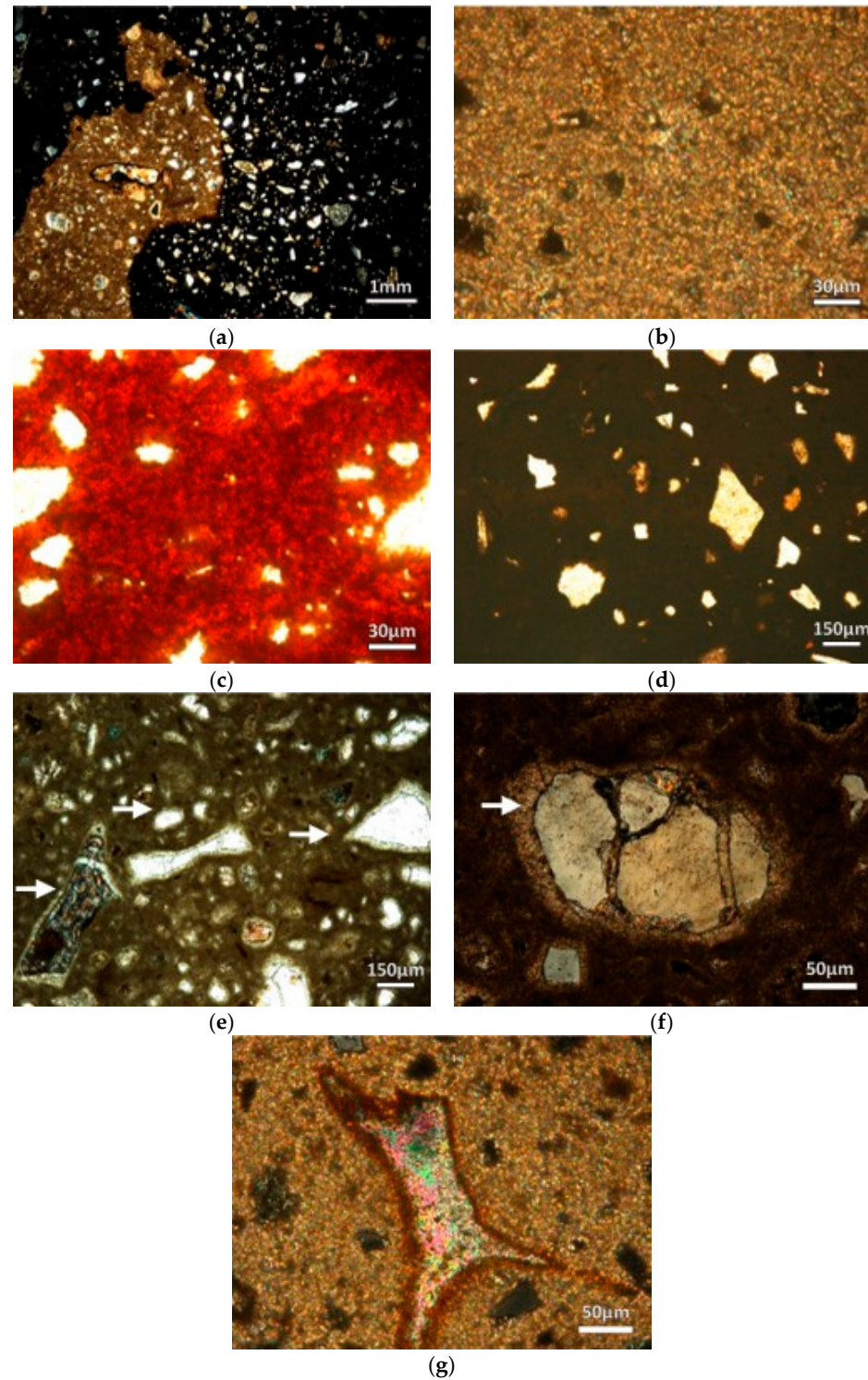


Figure 6. Photomicrographs of concretions. (a) A photomicrograph showing two matrices: light-colored and dark-colored matrices (2× objective used, scale bar = 1 mm and cross-polar light (XPL)); (b) Light-colored matrix with higher magnification, exhibiting high birefringence (60×, scale bar = 30 µm and XPL); (c) Dark-colored matrix with higher magnification with high light intensity (60×, scale

bar = 30 μm and XPL); (d) Grains enclosed in dark matrices showing absence of grain coating (10 \times objective, scale bar = 150 μm , plane polar light (PPL)); (e) Grains enclosed in light colored matrices coated with carbonate (indicated by arrows; 10 \times objective, scale bar = 150 μm , PPL); (f) A quartz grain enclosed in light-colored matrix with grain coating (indicated by an arrow) and displacive overgrowth of carbonate mineral (40 \times , scale bar = 50 μm and XPL); (g) Volcanic rock fragment replaced by carbonate mineral in light-colored matrix (40 \times , scale bar = 50 μm and XPL).

Major grains enclosed are quartz, feldspar, calcite, and volcanic rock fragments. The reddish brown and light gray matrices are referred to as “dark” and “light”, respectively, for the rest of this article. The dark concretion is composed of Fe-oxides (Figure 6c) and the light concretion is composed of Fe-enriched carbonate. Many grains within the light-colored matrices exhibit carbonate grain coatings (isopachous grain coating) (Figure 6e,f), whereas such grain coatings are absent in dark concretions (Figure 6d). Some calcite grains are relatively large and resemble volcanic glass (Figure 6g).

4.3.4. Fossil Bones

The marrow cavity of the femur (indeterminate dinosaur) is filled with a concretion similar to the concretion formed outside the bone (Figure 7a,b), containing similar grains, dark and light matrices, and grain coatings in the light matrix (Figure 7b). Concretion also fills the cavity of the rib (indeterminate dinosaur). Both the rib and femur samples include cortical (Figure 7c) and cancellous bones (Figure 7d).

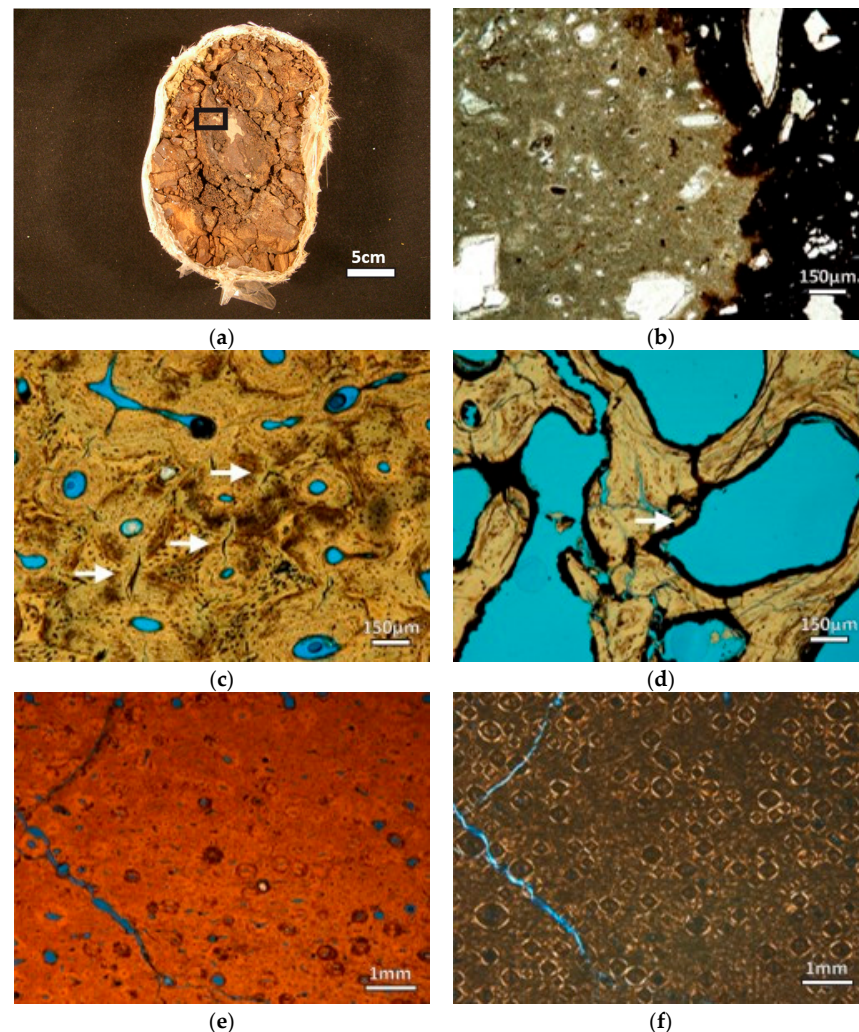


Figure 7. Cont.

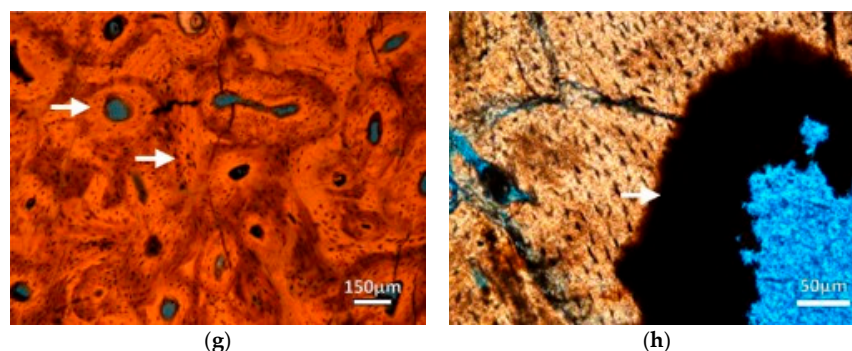


Figure 7. (a) Femur fragment after sawing (field of view is about 30 cm). The marrow cavity is filled with concretion, and the bone is crumbling because of the vibration from sawing. The black rectangle indicates the approximate location of the micrograph (b); (b) A photomicrograph of concretion filling the marrow cavity exhibiting similar characteristics to the concretion formed outside the bone. Dark matrix consists of Fe-oxides, and light matrix consists of Fe-enriched carbonate (10× objective, scale bar = 150 μm and plane polar light (PPL)); (c) A photomicrograph of a cortical bone of the femur showing preserved microstructures (10×, scale bar = 150 μm and PPL). Arrows point to radial fractures on the peripheral of osteon; (d) Cancellous bone of the femur showing authigenic mineral precipitation in the voids (10×, scale bar = 150 μm and PPL); (e) Photomicrograph of the cortical bone of femur showing general fabric (2×, scale bar = 1 mm and PPL); (f) Same part of the femur under cross-polarized light (2×, scale bar = 1 mm). Preserved lamellae are easily observed with cross-polarized light; (g) The arrow on top indicates an example of a Haversian canal, and the lower arrow indicates lacunae for osteocyte (10×, scale bar = 150 μm and PPL); (h) Close-up view of the pore within cortical bone. An arrow indicates opaque mineral precipitation inside the Haversian canal (40×, scale bar = 50 μm and PPL).

Preserved bone microstructures include osteonal lamellae (Figure 7e,f), Haversian canals (Figure 7g), and lacunae for osteocytes (Figure 7g). The radial cracks on the peripheral secondary osteon (Figure 7g) are indicative of the expansion of collagen [35], and there are no fractures cross-cutting these preserved microstructures. Smaller cavities in the cancellous bone and Haversian canals in the cortical bone remain mostly empty. However, these cavities exhibit evidence for authigenic mineral precipitation (Figure 7h).

4.4. Stable Isotope Geochemistry

Although dark- and light-colored concretions occur together within bone-bearing sandstone, $\delta^{13}\text{C}$, and $\delta^{18}\text{O}$ values of light-colored concretions are much higher than that of dark-colored concretions (9.1‰ and 9.5‰, respectively). The $\delta^{13}\text{C}$ value of the spheroidal concretion from channel sandstone is much lower than the concretions from bone-bearing sandstone. The isotopic compositions of cancellous and cortex bones are similar.

5. Discussion

5.1. Concretions in Bone-Bearing Sandstone

Carbonate concretions were present both in bone-bearing sandstone and channel sandstone. The concretions in bone-bearing sandstone include three phases of carbonate: (1) grain coating, (2) light-colored matrices, and (3) dark-colored matrices. Grain coating on sand grains exhibits isopachous fabric perpendicular to the grains and covers entire grains (Figure 6e). Isopachous grain coating forms in the phreatic zone, and as grain coatings are preserved in larger cement, the formation of grain coating predates the formation of concretion.

Concretions in bone-bearing sandstone are associated with large fossils; concretions are formed on the external surface of the large bones as well as in a large cavity (i.e., marrow cavity) of large bones. Petrography shows that early grain coatings were preserved in light colored matrices, yet they were absent on grains in dark colored matrices (Figure 6a).

Initially, light-colored matrices were interpreted as siderite, and dark-colored matrices were interpreted as Fe-oxides, resulting from the oxidation of Fe-enriched carbonate. However, the dark-colored matrices are highly effervescent with hydrochloric acid and contain carbonate minerals. The stable isotope composition difference between light-colored and dark-colored matrices (Table 1) indicates that the difference in appearance is not due to the staining. Instead, carbonate mineral in concretion re-equilibrated their isotopic composition with pore fluid during alteration.

Table 1. Stable isotope compositions of concretions and fossilized bones.

Sample	$\delta^{13}\text{C}$ (VPDB)	$\delta^{18}\text{O}$ (VSMOW)
Dark Concretion	−7.5	16.4
Light Concretion	2.1	25.9
Spheroidal Concretion	−22.4	17.8
Cortex Bone	−4.4	20.6
Cancellous Bone	−4.1	20.5

The $\delta^{13}\text{C}$ and $\delta^{18}\text{O}$ values of light-colored matrices are 9.1‰ and 9.5‰ higher than that of dark-colored matrices, contradicting the inverse enrichment/depletion trend in concretions from previous studies [15,36,37]. Additionally, the $\delta^{18}\text{O}$ value of dark matrices (16.4‰ VSMOW) is exceptionally low compared to the previous studies. Marchand et al. [38] reported that $\delta^{18}\text{O}$ of quartz cement precipitated in 1.5 to 3.0 km (60–90 °C) was ~7 to 9 ‰ lower than the $\delta^{18}\text{O}$ of quartz precipitated in shallower burial depth. As such, the low $\delta^{18}\text{O}$ of dark matrices may be a result of mesogenetic alteration of original carbonate concretion.

5.2. Concretion in Channel Sandstone

Concretion in the channel sandstone was not associated with fossils. No distinctive nucleation sites were found when the concretions were cut, and some concretions were found with a rim of sulfur. The $\delta^{13}\text{C}$ of concretion from channel sandstone is exceptionally low (−22.4‰). Such a low $\delta^{13}\text{C}$ composition in calcite is often associated with microbial sulfate reduction of organic material in shallow burial [15,39]. However, the channel sandstone in this study does not include any other carbonate phase, and petrography indicates that carbonate precipitated in early diagenesis, including calcite crystals that displaced biotite fabric and are not preserved (Figure 5b). Therefore, spheroidal concretion in channel sandstone likely formed during telogenesis.

5.3. Potential Impact on Fossil Preservation

Bone microstructures were well preserved in this study, and no biological modification or polygonal cracks were observed. Some radial fractures were found on the peripherals of osteons (Figure 7c), which are indicative of collagen hydration in the earliest stage of diagenesis [33,40]. Jans et al. [41] reported that microbial attack is very common among archaeological bones regardless of climate. However, Trueman and Martill [42] state that such structures (e.g., microbial/fungal boring and tunnels) are very rare among fossilized bones (N = 350) spanning more than 350 million years and covering a wide range of depositional environments. No sign of microbial modification of the bone was found in petrographic analysis in this study, which may suggest that the physicochemical environment in early burial inhibited microbial activities. Small cavities, including the Haversian canal and pores in cancellous bone, are lined with clay and Fe-oxide (Figure 7d,h), yet carbonate precipitation was limited to the large cavity (marrow cavity) and external surface of the bones. Parts of fossilized bones were also replaced with Fe-oxides (Figure 7h). The earliest event recorded in the host rock was a carbonate grain coating preserved in a concretion. Grain coating was not preserved in the channel sandstone, yet splitting biotite grains suggests displacive overgrowth of calcite in eogenesis [43]. As such, early precipitation of calcite on the surface of the bones cannot be ruled out.

Stable isotope compositions of the cortex and cancellous bones did not show similarity to any of the concretions, suggesting dinosaur bones did not re-equilibrate stable isotope compositions with the pore fluid that formed concretions. The stable isotope compositions of structural carbonate from fossil bones and teeth are utilized for paleoecological investigation, e.g., [6,9,19]. Thus, results from this study can support the authenticity of the stable isotope compositions in previous investigations. Among concretions in this study, the precipitation of the light-colored concretion was the earliest to form (see the previous section) However, both $\delta^{13}\text{C}$ and $\delta^{18}\text{O}$ of the concretions were ~ 5 and 7% higher, respectively, than those of fossil bones. Stable isotope compositions of fossils in this study are comparable to previously reported values of herbivorous dinosaur bones from the Hell Creek Formation [19]. Although multiple generations of carbonate precipitation take place in a host rock, stable isotope compositions of concretions suggest that fractionation between fossils and pore fluid is limited.

Preservation of grain coating in light-colored matrices suggests that limited interaction with pore fluid through the formation of concretion aids in preserving early diagenetic signals. Concretions cover fossils only partially, and detrital grains are enclosed in marrow cavities. As such, fossil bones were not fully isolated from the pore fluid during later diagenesis (meso- and telogenesis). Additionally, smaller bones were preserved without any association with concretion. Thus, the formation of concretion may have a limited impact on fossil preservation in this assemblage. Alternatively, formation of concretions may have limited the interaction between pore fluid and fossil bones by taking up ions. Further geochemical analysis using advanced techniques including inductively coupled plasma mass spectrometry (ICP-MS) would be useful to test such a hypothesis [44].

Although spheroidal concretion in this study was not associated with any fossils, these concretions hold unique evidence for carbonate precipitation during telogenesis. Based on the isotopic composition of spheroidal concretion ($\delta^{13}\text{C} = -22.4\%$), isotopic fractionation between telogenic pore fluid and fossilized bones is not evident.

6. Conclusions

Four distinctive carbonate phases were observed in the bone-bearing sandstone and the channel sandstone below: (1) grain coating, (2,3) light- and dark-colored matrices of concretion from the bone-bearing sandstone, and (4) spheroidal concretion from the channel sandstone. Based on the morphology and stable isotopic compositions of these carbonate minerals, early carbonate precipitation took place in the phreatic zone during eogenesis. These concretions preserved early diagenetic signals such as grain coating, yet part of the concretion was altered during the mesogenesis. The spheroidal concretion from the channel sandstone is distinctive from the concretions in bone-bearing sandstone based on its morphology and stable isotopic composition; the extremely low $\delta^{13}\text{C}$ value suggests that microbial sulfate reduction was associated with the formation of this concretion. In addition to the carbonate phases, fabric of the sandstone, altered grain, and partial-full dissolution of grains indicate evolving pore-fluid geochemistry.

Fossilized bones analyzed in this study exhibited well-preserved microstructures. The marrow cavity was permineralized with carbonate cement mixed with detrital grains, suggesting fossils in this study were susceptible to pore fluid interaction. Although small pores were not fully permineralized, authigenic minerals such as clay and oxide were observed. Despite the evidence of pore fluid interaction, stable isotopic compositions of these bones were dissimilar to concretions, suggesting that isotopic fractionation between pore fluid and fossil bone minerals was limited.

Although these carbonate phases record unique diagenetic conditions, concretions do not seem to enhance the preservation of the skeletal remains. Instead, early carbonate precipitation evidenced by grain coating likely contributed to the isolation of bones in early diagenesis [44]. Additionally, various carbonate phases can aid in deciphering the diagenetic conditions skeletal remains experienced. The results from this study can be incorporated into experimental designs for actual experiments. Although altered feldspar

and other detrital grains were observed, clay minerals were not analyzed in this study. As clay minerals are products of such alteration, further investigation into clay minerals may provide more detail on the diagenetic history of the Hell Creek Formation.

Petrography and stable isotope analysis were useful for interpreting carbonate precipitated in different diagenetic stages, yet other techniques including Inductivity Coupled Plasma Mass Spectrometry (ICP-MS) may help decipher more detailed diagenetic history [44]. Thus, ICP-MS may be added in future investigations.

Funding: This research was funded by the Geological Society of America, Graduate Research Grant (2012) and Sigma Xi, Grant-in-Aid of Research (2014).

Data Availability Statement: All data generated by this study are available in this manuscript.

Acknowledgments: I would like to thank J. G. Schmitt for advising the initial research, C. A. Suarez for stable isotope discussion, E. Pollock and L. Conaway of UASIL for assistance in stable isotope analysis, staff at the Makoshika State Park for field accommodations, MSSE Field Paleontology students for field assistance, and the reviewers for their constructive feedback.

Conflicts of Interest: The author declares no conflict of interest.

Appendix A.

Appendix A.1. Depositional Environment Interpretation

The lithofacies classification of Miall ([45], p.79) is adopted to this study in order to avoid biased interpretation. The lithofacies and brief interpretations are summarized in Table A1. The lithofacies identified in the studied stratigraphic section include trough cross-stratified sandstone (lithofacies: St), massive sandstone (lithofacies: Sm), massive mudrock (lithofacies: Fm), interlaminated very fine-grained sandstone and mudrock (lithofacies: Fl), and coal (lithofacies: C).

Table A1. Lithofacies and interpretation.

Code	Facies	Sedimentary Structure	Interpretation
St	Sand; very fine to medium	Grouped trough cross-lamination	Migration of 3D dunes
Sm	Sand; very fine to fine	Massive or faint lamination	Suspension settling, bioturbated
Fl	Sand, Silt and Mud	Fine wavy lamination	Suspension settling, weak traction current
Fm	Mud, silt	Massive	Suspension settling, bioturbated
C	Coal	Plant, mud films	Standing body of water, low sediment input

Appendix A.2. Trough Cross-Stratified Sandstone

The trough cross-stratified sandstone in the study area comprises moderately sorted medium-grained sand. Grains are angular to sub-angular and include minor amounts (5%–10%) of mafic minerals and volcanic rock fragments. The sedimentary structures seen in the trough cross-stratified sandstone are cosets of mutually cross-cutting troughs. The angle of trough-cross lamination ranges from 5 to 20°. The thickness of each stratification is about 2 mm, and the thickness of cosets ranges from 15 to 30 cm. Additionally, the trough cross-stratified sandstone is grain-supported with tangential grain contacts, highly porous and very friable.

Discrete coal stringers mms to cms in thickness and up to 50 cm in length are present. The coal stringers are oriented along the slope of trough cross-lamination. The trough cross-stratified sandstone also includes small (1–5 cm) spheroidal bodies; some are friable

and yellow to tan in color, and others are well cemented and reddish brown in color (i.e., concretion). Such cemented bodies, however, exhibit a light gray color on freshly broken surfaces, and broken surfaces react with an acid (0.1 M HCl). Vertebrate fossils were absent in the trough cross-stratified sandstone in the outcrop studied. The presence of trough cross-stratified sandstone beds is very common in sandstone units throughout the study area, and each bed is laterally discontinuous.

Trough cross-stratification is formed by migration of 3D dunes, which develop under lower flow regime conditions [46]. Based on their orientation, the coal stringers represent plant material deposited on the lee side of dunes. Since the original depositional structure (i.e., cross-stratification) is observed in the spheroidal bodies, both friable and well-cemented spheroidal bodies are likely products of diagenesis. The absence of vertebrate remains in the basal sandstone may not have any significance since other cross-stratified sandstone beds in the study area yield fossils.

Appendix A.3. Massive Sandstone (Lithofacies: Sm)

Massive sandstone in the study area comprises poorly sorted fine- to very fine-grained sand and mud. Grains are sub-angular and include a minor amount (10%) of mafic minerals and volcanic rock fragments. Sedimentary structures or root casts are not preserved in the massive sandstone; only a few faint wavy laminations are observed. The color of massive sandstone is light gray to tan due to its high clay content. The massive sandstones include smaller bodies of different colored matrices; the color of such bodies ranges from yellow to light brown and often has an oxidized appearance.

Coal is present either as discrete fragments (up to 5 mm) or as stringers (up to centimeters thick and decimeters in length). Partially coalified plant fossils (leaves and pine cones) are also present in the massive sandstone. Vertebrate fossils are only present in the massive sandstone labeled as the bone-bearing sandstone on the stratigraphic column. Spheroidal concretions found in the trough cross-stratified sandstone are absent in massive sandstone beds; the only concretions in the bone-bearing sandstone occur around fossil bones. Massive sandstone (Sm) beds are about 1m thick and occur between massive mudrock (Fm) beds. Both upper and lower contacts between massive sandstone and massive mudrock are gradational.

The fine sand-sized grains and high mud content suggest the massive sandstone was deposited in a low-energy setting. The massive sandstone beds can occur as a result of bank collapse in a small channel [47] or due to post-depositional modification ([45], p. 123). The massive sandstone beds do not occur adjacent to channel sandstone in this section. Hence, these massive sandstone beds are not likely bank collapse deposits. In contrast, the presence of vertebrate fossils and coal stringers suggests post-depositional modification by biological activity (i.e., bioturbation); hence, the massive fabric is interpreted as a result of post-depositional modification. Fine sand and high mud content suggest that the depositional environment was a low-energy setting.

Appendix A.4. Massive Mudrock (Lithofacies: Fm)

Massive mudrock consists of light- to dark-gray clay and silt. Sedimentary structures or root structures are not preserved in the massive mudrock; however, few faint laminations are observed in silty beds. Such laminations are rare and only partially preserved. Coal is present either as stringers (up to centimeters thick and decimeters in length) or as small discrete fragments (up to 5 mm), and the coal content varies widely among the mudrock beds. Paleosols were very poorly developed in all the mudrock beds. The mudrock beds adjacent to coal beds exhibit a gradational increase in coal content toward the coal beds, which makes the contact between mudrock and coal beds gradational. No vertebrate fossils were found in the massive mudrock beds. Bed thickness ranges from 20 cm to 1 m and gradually decreases in frequency toward the top of the outcrop.

Massive mud deposits are a result of suspension settling in a standing body of water [48]. In a fluvial setting, massive mud is deposited on a distal floodplain during flooding

or in standing pools of water such as floodplain ponds and swamps [48]. The gray color of the mudrock and abundant plant debris are indicative of a poorly drained overbank environment ([49], p. 66). Partially preserved faint wavy lamination suggests ripple lamination was present prior to bioturbation. The presence of ripple lamination is indicative of lower flow regime conditions [50].

Appendix A.5. Interlaminated Very Fine-Grained Sandstone and Mudrock (Lithofacies: Fl)

Interlaminated very fine-grained sandstone and mudrock consist of brown to gray mudrock and very fine-grained gray sandstone. The contact between interlamination is gradational and partly obscure. The color of the mudrock in the bottom half is mostly gray with thin (up to 5 cm) layers of brown mudrock, whereas the mudrock in the upper half is mostly brown in color. Some silty mudrock exhibits faint wavy laminations. The lithology of the sandstone is similar to other massive sandstone (lithofacies: Sm) beds, structureless gray mud-rich sandstone. The occurrence and thickness of sandstone subunits gradually decrease toward the top. Interlaminated very fine-grained sandstone and mudrock overlie the basal trough cross-stratified sandstone (lithofacies: St) and are overlain by a coal bed.

Interlamination of mud and very fine sand represents deposition from suspension and from weak traction currents ([45], p. 84). Faint wavy lamination suggests the presence of ripple cross-lamination, which is indicative of lower flow regime conditions. The color of the mudrock suggests the upper half was deposited in a well-drained environment ([49], p. 66). A decrease in sand content toward the top may suggest a channel migration and succession toward a distal floodplain environment.

Appendix A.6. Lignitic Coal (Lithofacies: C)

Lignitic coal layers occur frequently in the Hell Creek and overlying Tullock Formations in the study area. Two lignitic coal beds were included in the sedimentary sequence studied, and both beds were stratigraphically lower than the K-Pg boundary. The lignitic coal layers are interlaminated with dark gray clay and laterally discontinuous. Lignitic coal beds overlie lithofacies Fl and Fm with gradational contact.

Whereas autochthonous peats and coals directly overlie paleosols, allochthonous coals lack an associated underlying paleosol and accumulated in a body of still water as detrital organic matter or as a floating peat layer [49]. Since the lignitic coal facies overlie a massive mudrock (lithofacies: Fm) and interlaminated very fine-grained sandstone and mudrock (lithofacies: Fl) in the sedimentary sequence studied, such coal facies are interpreted as a peat swamp deposit. McCabe [51] suggested that the presence of coal indicates the presence of raised peat swamps undergoing rapid plant accumulation under humid tropical conditions.

Appendix A.7. Facies Association

The outcrop studied comprises five lithofacies; St, Sm, Fl, Fm, and C. The measured section includes two facies associations: facies association (FA) 1 and 2. FA 1 includes lithofacies St overlain by Fl and C, whereas FA2 includes repeating sequences of lithofacies Sm and Fm.

Appendix A.8. Facies Association 1

Facies association (FA) 1 is defined by a trough cross-stratified sandstone (St) overlain by an interlaminated very fine sandstone and mudrock (Fl) and lignitic coal (C). The coal content within the lithofacies Fl gradually increases toward the top (contact between lignitic coal). The upper contact of FA 1 is marked by lignitic coal facies (C), and the contact between FA 1 and FA 2 is gradational. The lower contact of FA 1 is not exposed. The contact between lithofacies St and Fl is gradational; the lowermost lamina in the overlying lithofacies Fl consists of gray very fine sand and silt. The sequence is 4.5m thick and fines upward into lithofacies Fl and C. Lithofacies C contains dark gray mud, which differs from

the underlying mudrock (part of lithofacies: Fl). FA 1 is only present at the base of the outcrop studied.

Previous studies [22,28] state the Hell Creek Formation was deposited in a fluvial setting. In a fluvial setting, migrations of 3D dunes take place in a channel [50]; hence, the cosets of lithofacies St are interpreted as a channel sandstone (architectural element CH). Although fining upward grain size and gradual contact with lithofacies Fl suggests lateral migration of the channel, further interpretation (i.e., lateral-accretion versus downstream-accretion macroform) requires additional information such as the geometry of the sandstone bed. Interlaminated very fine sandstone and mudrock (lithofacies: Fl) rest directly above a channel sandstone (lithofacies: St). The gradational contact between the lithofacies Fl and St and the increase in coal content within Fl suggest a gradual loss of kinetic energy in the depositional system, such as channel migration or abandonment. Based on the close association with channel sandstone and gradational contact, lithofacies Fl is interpreted as a levee deposit (architectural element: LV). Lignitic coal in a fluvial deposit is interpreted as a swamp deposit [51] and is indicative of a poorly drained environment. In contrast, the brown color of mud in Fl is indicative of well-drained overbank deposits ([49], p. 66).

Based on the presence of channel, levee, and floodplain deposits, FA 1 is interpreted as a sequence recording channel migration. Channel migrations forming levee deposits represent sedimentary events with a duration of 10^2 to 10^3 years [45]; hence, the Fl unit may represent 10^2 to 10^3 years.

Appendix A.9. Facies Association 2

Facies association (FA) 2 is defined by repeating sequences of massive sandstone (Sm) and massive mudrock (Fm). The total thickness of this sequence is 6.4m, and both top and bottom boundaries are defined by lignitic coal facies (C). Boundaries between Sm and Fm are gradational. The thickness of each bed gradually decreases toward the top of this sequence. Differential weathering due to the relatively resistant sandstone beds (Sm) produced a gentle slope in the middle of the hill. The overall sequence of the FA 2 exhibits a fining upward trend in grain size.

Crevasse splays form lobate sheets of sand that prograde into a wetland environment and are common features of the fluvial depositional system [52]. Studies of modern anastomosing systems [52] also indicate that multiple stacked splay sequences separated by mud are common. Therefore, FA2 is interpreted as a series of crevasse splay deposits based on the presence of multiple fine-grained sandstone beds (Sm) interbedded with mudrock beds (Fm).

Crevasse splay sandstone (architectural element: CS) often exhibits trough cross-stratification or ripple cross-lamination [45], and the lack of such stratifications is likely due to bioturbation suggested by the presence of plant material and fossils. Massive mudrock (Fm) can be deposited on a distal flood plain [53]. However, close association with crevasse splay sandstone suggests Fm was deposited on a distal floodplain (architectural element: FF).

Appendix A.10. Overall Interpretation

The local thickness of the Hell Creek Formation in the Glendive area is estimated to be 99 m [25], and the Hell Creek Formation represents depositional events of 1.36 to 2.5 million years [26,27]. Based on these data, the 11m sequence may represent 151,000 to 278,000 years.

The overall sequence (a series of crevasse splays overlying a channel migration sequence) is interpreted as an alluvial succession from a channel to an overbank with occasional breaching of levees. Levees and crevasse splays tend to have higher rates of deposition in comparison to distal floodplains [54]; hence, the time represented by Fm is greater where the thicknesses are comparable. The lack of paleosol horizons may suggest that sedimentary accumulation was relatively fast throughout the sequence.

References

1. Schweitzer, M.H.; Wittmeyer, J.L.; Horner, J.R. Soft Tissue and Cellular Preservation in Vertebrate Skeletal Elements from the Cretaceous to the Present. *Proc. R. Soc. B* **2007**, *274*, 183–197. [[CrossRef](#)] [[PubMed](#)]
2. Pan, Y.; Zheng, W.; Moyer, A.E.; O'Connor, J.K.; Wang, M.; Zheng, X.; Wang, X.; Schroeter, E.R.; Zhou, Z.; Schweitzer, M.H. Molecular Evidence of Keratin and Melanosomes in Feathers of the Early Cretaceous Bird *Eoconfuciusornis*. *Proc. Natl. Acad. Sci. USA* **2016**, *113*, E7900–E7907. [[CrossRef](#)] [[PubMed](#)]
3. Bailleul, A.M.; Zheng, W.; Horner, J.R.; Hall, B.K.; Holliday, C.M.; Schweitzer, M.H. Evidence of Proteins, Chromosomes and Chemical Markers of DNA in Exceptionally Preserved Dinosaur Cartilage. *Natl. Sci. Rev.* **2020**, *7*, 815–822. [[CrossRef](#)] [[PubMed](#)]
4. Brown, C.M.; Henderson, D.M.; Vinther, J.; Fletcher, I.; Sistiaga, A.; Herrera, J.; Summons, R.E. An Exceptionally Preserved Three-Dimensional Armored Dinosaur Reveals Insights into Coloration and Cretaceous Predator-Prey Dynamics. *Curr. Biol.* **2017**, *27*, 2514–2521.e3. [[CrossRef](#)]
5. Wiemann, J.; Menéndez, I.; Crawford, J.M.; Fabbri, M.; Gauthier, J.A.; Hull, P.M.; Norell, M.A.; Briggs, D.E.G. Fossil Biomolecules Reveal an Avian Metabolism in the Ancestral Dinosaur. *Nature* **2022**, *606*, 522–526. [[CrossRef](#)]
6. Kohn, M.J.; McKay, M.P.; Knight, J.L. Dining in the Pleistocene—Who's on the Menu? *Geology* **2005**, *33*, 649–652. [[CrossRef](#)]
7. Heuser, A.; Tütken, T.; Gussone, N.; Galer, S.J.G. Calcium Isotopes in Fossil Bones and Teeth—Diagenetic versus Biogenic Origin. *Geochim. Cosmochim. Acta* **2011**, *75*, 3419–3433. [[CrossRef](#)]
8. Cullen, T.M.; Longstaffe, F.J.; Wortmann, U.G.; Huang, L.; Fanti, F.; Goodwin, M.B.; Ryan, M.J.; Evans, D.C. Large-Scale Stable Isotope Characterization of a Late Cretaceous Dinosaur-Dominated Ecosystem. *Geology* **2020**, *48*, 546–551. [[CrossRef](#)]
9. Suarez, C.A.; Ludvigson, G.A.; Gonzalez, L.A.; Fiorillo, A.R.; Flaig, P.P.; McCarthy, P.J. Use of Multiple Oxygen Isotope Proxies for Elucidating Arctic Cretaceous Palaeo-Hydrology. *Geol. Soc. Lond. Spec. Publ.* **2013**, *382*, 185–202. [[CrossRef](#)]
10. Passey, B.H.; Levin, N.E. Triple Oxygen Isotopes in Meteoric Waters, Carbonates, and Biological Apatites: Implications for Continental Paleoclimate Reconstruction. *Rev. Mineral. Geochem.* **2021**, *86*, 429–462. [[CrossRef](#)]
11. Morad, S. Carbonate Cementation in Sandstones: Distribution Patterns and Geochemical Evolution. In *Carbonate Cementation in Sandstones*; Morad, S., Ed.; Wiley: Hoboken, NJ, USA, 1998; pp. 1–26, ISBN 978-0-632-04777-2.
12. Cope, J.C.W.; Curtis, C.D. Palaeobiology Meets Geochemistry: Concretions as Tombs. *J. Geol. Soc.* **2000**, *157*, 163–164. [[CrossRef](#)]
13. Kendall, C.; Eriksen, A.M.H.; Kontopoulos, I.; Collins, M.J.; Turner-Walker, G. Diagenesis of Archaeological Bone and Tooth. *Palaeogeogr. Palaeoclimatol. Palaeoecol.* **2018**, *491*, 21–37. [[CrossRef](#)]
14. Schweitzer, M.H.; Johnson, C.; Zocco, T.G.; Horner, J.R.; Starkey, J.R. Preservation of Biomolecules in Cancellous Bone of Tyrannosaurus Rex. *J. Vertebr. Paleontol.* **1997**, *17*, 349–359. [[CrossRef](#)]
15. Mozley, P.S.; Burns, S.J. Burns Oxygen and Carbon Isotopic Composition of Marine Carbonate Concretions: An Overview. *J. Sediment. Res.* **1993**, *63*, 73–83. [[CrossRef](#)]
16. Hedges, R.E.M. Bone Diagenesis: An Overview of Processes. *Archaeometry* **2002**, *44*, 319–328. [[CrossRef](#)]
17. Boggs, S. *Principles of Sedimentology and Stratigraphy*; Pearson Prentice Hall: Upper Saddle River, NJ, USA, 2006; p. 662.
18. Ullmann, P.V.; Pandya, S.H.; Nelleremoe, R. Patterns of Soft Tissue and Cellular Preservation in Relation to Fossil Bone Tissue Structure and Overburden Depth at the Standing Rock Hadrosaur Site, Maastrichtian Hell Creek Formation, South Dakota, USA. *Cretac. Res.* **2019**, *99*, 1–13. [[CrossRef](#)]
19. Fricke, H.C.; Pearson, D.A. Stable Isotope Evidence for Changes in Dietary Niche Partitioning among Hadrosaurian and Ceratopsian Dinosaurs of the Hell Creek Formation, North Dakota. *Paleobiology* **2008**, *34*, 534–552. [[CrossRef](#)]
20. Doring, M.A.; Smit, J.; Voeten, D.F.; Berruyer, C.; Tafforeau, P.; Sanchez, S.; Stein, K.H.; Verdegaal-Warmerdam, S.J.; van der Lubbe, J.H. The Mesozoic Terminated in Boreal Spring. *Nature* **2022**, *603*, 91–94. [[CrossRef](#)]
21. Belt, E.S.; Hicks, J.F.; Murphy, D.A. A Pre-Lancian Regional Unconformity and Its Relationship to Hell Creek Paleogeography in South-Eastern Montana. *Rocky Mt. Geol.* **1997**, *31*, 1–26.
22. Fastovsky, D.E. Paleoenvironments of Vertebrate-Bearing Strata during the Cretaceous-Paleogene Transition, Eastern Montana and Western North Dakota. *Palaios* **1987**, *2*, 282. [[CrossRef](#)]
23. Johnson, K.R.; Hickey, L.J. Megafloal Change across the Cretaceous/Tertiary Boundary in the Northern Great Plains and Rocky Mountains, U.S.A. In *Geological Society of America Special Papers*; Geological Society of America: Boulder, CO, USA, 1990; Volume 247, pp. 433–444, ISBN 978-0-8137-2247-4.
24. Hartman, J.H.; Butler, R.D.; Weiler, M.W.; Schumaker, K.K.; Wilson, G.; Clemens, W.; Horner, J. *Context, Naming, and Formal Designation of the Cretaceous Hell Creek Formation Lectostratotype, Garfield County, Montana*; Geological Society of America Special Paper; Geological Society of America: Boulder, CO, USA, 2014; Volume 503.
25. Zaleha, M.J. The Hell Creek Formation (Maastrichtian), Glendive Area, Montana: Sedimentology, Paleoenvironments, and Provenance and Their Stratigraphic and Taphonomic Implications. Ph.D. Thesis, Ohio University, Athens, OH, USA, 1988.
26. Hicks, J.F.; Johnson, K.R.; Obradovich, J.D.; Tauxe, L.; Clark, D.; Hartman, J. Magnetostratigraphy and Geochronology of the Hell Creek and Basal Fort Union Formations of Southwestern North Dakota and a Recalibration of the Age of the Cretaceous-Tertiary Boundary. *Geol. Soc. Am. Spec. Pap.* **2002**, *361*, 35–55.
27. Lund, S.P.; Hartman, J.H.; Banerjee, S.K. Magnetostratigraphy of Interfingering Upper Cretaceous–Paleocene Marine and Continental Strata of the Williston Basin, North Dakota and Montana. In *The Hell Creek Formation and the Cretaceous-Tertiary Boundary in the Northern Great Plains: An Integrated Continental Record of the End of the Cretaceous*; Geological Society of America: Boulder, CO, USA, 2002; ISBN 978-0-8137-2361-7.

28. Sheehan, P.M.; Fastovsky, D.E.; Hoffmann, R.G.; Berghaus, C.B.; Gabriel, D.L. Sudden Extinction of the Dinosaurs: Latest Cretaceous, Upper Great Plains, USA. *Science* **1991**, *254*, 835–839. [[CrossRef](#)] [[PubMed](#)]
29. Fastovsky, D.E.; Bercovici, A. The Hell Creek Formation and Its Contribution to the Cretaceous–Paleogene Extinction: A Short Primer. *Cretac. Res.* **2016**, *57*, 368–390. [[CrossRef](#)]
30. Johnson, K.R.; Nichols, D.J.; Hartman, J.H. Hell Creek Formation: A 2001 Synthesis. *Geol. Soc. Am. Spec. Pap.* **2002**, *361*, 503–510.
31. Fowler, D. The Hell Creek Formation, Montana: A Stratigraphic Review and Revision Based on a Sequence Stratigraphic Approach. *Geosciences* **2020**, *10*, 435. [[CrossRef](#)]
32. Surdam, R.C.; MacGowan, D.B.; Dunn, T.L. Diagenetic Pathways of Sandstone and Shale Sequences. *Rocky Mt. Geol.* **1989**, *27*, 21–31.
33. Hagen, E.S.; Surdam, R.C. Thermal Evolution of Laramide-Style Basins: Constraints from the Northern Bighorn Basin, Wyoming and Montana. In *Thermal History of Sedimentary Basins*; Naeser, N.D., McCulloh, T.H., Eds.; Springer: New York, NY, USA, 1989; pp. 277–295, ISBN 978-1-4612-8124-5.
34. Koch, P.L.; Tuross, N.; Fogel, M.L. The Effects of Sample Treatment and Diagenesis on the Isotopic Integrity of Carbonate in Biogenic Hydroxylapatite. *J. Archaeol. Sci.* **1997**, *24*, 417–429. [[CrossRef](#)]
35. Pfretzschner, H.-U. Collagen Gelatinization: The Key to Understand Early Bone-Diagenesis. *Palaeontogr. Abt. A Palaeozool.* **2006**, *278*, 135–148. [[CrossRef](#)]
36. Coniglio, M.; Myrow, P.; White, T. Stable Carbon and Oxygen Isotope Evidence of Cretaceous Sea-Level Fluctuations Recorded in Septarian Concretions from Pueblo, Colorado, U.S.A. *J. Sediment. Res.* **2000**, *70*, 700–714. [[CrossRef](#)]
37. Smith, M.E.; McNeill, D.F.; Murray, S.T.; Swart, P.K. Internal Isotopic Variability of Neogene Carbonate Concretions: Constraining Formational Growth Mechanisms and Isotopic Disequilibrium. *Sedimentology* **2023**, *70*, 1553–1579. [[CrossRef](#)]
38. Marchand, A.M.E.; Macaulay, C.I.; Haszeldine, R.S.; Fallick, A.E. Pore Water Evolution in Oilfield Sandstones: Constraints from Oxygen Isotope Microanalyses of Quartz Cement. *Chem. Geol.* **2002**, *191*, 285–304. [[CrossRef](#)]
39. Gautier, D.L.; Claypool, G.E. *Interpretation of Methanic Diagenesis in Ancient Sediments by Analogy with Processes in Modern Diagenetic Environments: Part 1. Concepts and Principles*; American Association of Petroleum Geologists: Tulsa, OK, USA, 1984.
40. Pfretzschner, H.-U.; Tütken, T. Rolling Bones–Taphonomy of Jurassic Dinosaur Bones Inferred from Diagenetic Microcracks and Mineral Infillings. *Palaeogeogr. Palaeoclimatol. Palaeoecol.* **2011**, *310*, 117–123. [[CrossRef](#)]
41. Jans, M.M.E.; Nielsen-Marsh, C.M.; Smith, C.I.; Collins, M.J.; Kars, H. Characterisation of Microbial Attack on Archaeological Bone. *J. Archaeol. Sci.* **2004**, *31*, 87–95. [[CrossRef](#)]
42. Trueman, C.N.; Martill, D.M. The Long-Term Survival of Bone: The Role of Bioerosion. *Archaeometry* **2002**, *44*, 371–382. [[CrossRef](#)]
43. Braithwaite, C.J.R. Displacive Calcite and Grain Breakage in Sandstones. *J. Sediment. Res.* **1989**, *59*, 258–266. [[CrossRef](#)]
44. Bosio, G.; Gioncada, A.; Gariboldi, K.; Bonaccorsi, E.; Collareta, A.; Pasero, M.; Di Celma, C.; Malinverno, E.; Urbina, M.; Bianucci, G. Mineralogical and Geochemical Characterization of Fossil Bones from a Miocene Marine Konservat-Lagerstätte. *J. S. Am. Earth Sci.* **2021**, *105*, 102924. [[CrossRef](#)]
45. Miall, A.D. *The Geology of Fluvial Deposits: Sedimentary Facies, Basin Analysis, and Petroleum Geology*; Springer: Berlin/Heidelberg, Germany, 2013.
46. Harms, J.C.; Southard, J.B.; Southard, J.B.; Walker, R.G. *Structure and Sequence in Clastic Rocks*; SEPM (Society for Sedimentary Geology): Claremore, OK, USA, 1982; ISBN 978-1-56576-238-1.
47. Jones, B.G.; Rust, B.R. Massive Sandstone Facies in The Hawkesbury Sandstone, A Triassic Fluvial Deposit Near Sydney, Australia. *J. Sediment. Res.* **1983**, *53*, 1249–1259. [[CrossRef](#)]
48. Miall, A.D. Architectural-Element Analysis: A New Method of Facies Analysis Applied to Fluvial Deposits. *Earth-Sci. Rev.* **1985**, *22*, 261–308. [[CrossRef](#)]
49. Reading, H.G. (Ed.) *Sedimentary Environments: Processes, Facies and Stratigraphy*; John Wiley & Sons: Hoboken, NJ, USA, 2009.
50. Miall, A.D. Lithofacies Types and Vertical Profile Models in Braided River Deposits: A Summary. 1977, pp. 597–604. Available online: https://archives.datapages.com/data/dgs/005/005001/597_cspgsp0050597.htm (accessed on 20 September 2024).
51. McCabe, P.J. Depositional Environments of Coal and Coal-Bearing Strata. In *Sedimentology of Coal and Coal-Bearing Sequences*; Rahmani, R.A., Flores, R.M., Eds.; Wiley: Hoboken, NJ, USA, 1985; pp. 11–42, ISBN 978-0-632-01286-2.
52. Collinson, J.D.; Lewin, J. (Eds.) *Anastomosed Fluvial Deposits: Modern Examples from Western Canada*. In *Modern and ancient fluvial systems*; Wiley: Hoboken, NJ, USA, 1983; pp. 155–168, ISBN 978-0-632-00997-8.
53. Rust, B.R. Depositional Models for Braided Alluvium. 1977, pp. 605–625. Available online: https://archives.datapages.com/data/dgs/005/005001/605_cspgsp0050605.htm (accessed on 20 September 2024).
54. Bridge, J.S. *Facies Models Revisited*; Posamentier, H.W., Walker, R.G., Eds.; SEPM (Society for Sedimentary Geology): Claremore, OK, USA, 2006; ISBN 978-1-56576-121-6.

Disclaimer/Publisher’s Note: The statements, opinions and data contained in all publications are solely those of the individual author(s) and contributor(s) and not of MDPI and/or the editor(s). MDPI and/or the editor(s) disclaim responsibility for any injury to people or property resulting from any ideas, methods, instructions or products referred to in the content.